# Excitation, Ionization, and Fragmentation of Chiral Molecules in Asymmetric Microenvironments: A Mass-Resolved R2PI Spectroscopic Study

**Susanna Piccirillo,[†] Flaminia Rondino,[‡] Daniele Catone,[‡] Anna Giardini Guidoni,[‡,§] Alessandra Paladini,[‡] Mario Tacconi,[‡] Mauro Satta,[§] and Maurizio Speranza*[,||]**

*Dipartimento di Scienze e Tecnologie Chimiche, Università degli Studi di Roma "Tor Vergata", Roma, Italy, Dipartimento di Chimica, Università degli Studi di Roma "La Sapienza", P.le A. Moro 5, 00185 Roma, Italy, CNR-IMIP (sezione Istituto Materiali Speciali), I-85050 Tito Scalo (Pz), Italy, and Facoltà di Farmacia, Dipartimento di Studi di Chimica e Tecnologia delle Sostanze Biologicamente Attive, Università degli Studi di Roma "La Sapienza", P.le A. Moro 5, 00185 Roma, Italy*

*Received: December 2, 2004; In Final Form: January 4, 2005*

One- and two-color, mass selected R2PI spectra of the $S_1 \leftarrow S_0$ transitions in the bare (*R*)-(+)-1-phenyl-1-propanol and its complexes with bidentate solvent molecules, like the (*R*)-(−)- and (*S*)-(+)-3-hydroxytetrahydrofuran enantiomers, have been recorded after a supersonic molecular beam expansion. The one-color R2PI excitation spectra of the diastereomeric complexes are characterized by three main peaks, one red-shifted and the other two blue-shifted relative to the band origin of the most stable anti conformer of the bare chromophore. The opposite direction of these spectral shifts is ascribed to the occurrence of three different hydrogen bonded isomeric structures for each individual complex, while their different magnitude depends on the configuration of the bidentate solvent molecule as well as its specific hydrogen bond interaction center, whether the ethereal oxygen atom or the hydroxyl group. The same factors play a major role in determining the magnitude of the phenomenological activation barriers for the loss of an ethyl radical from the ionized diastereomeric complexes.

## 1. Introduction

The biological functions of DNA are strictly related to its structural variability and flexibility which, in turn, depend on its base sequence and the environmental conditions.[1−3] The critical importance of DNA flexibility for its biological functions is apparent from structures of its complexes with proteins,[4] enzymes,[5−7] and drugs[8] in which the noncovalent interactions within the polynucleotide chain and between it and the specific partner play a crucial role.

A detailed understanding of the nature and the specificity of these weak interactions requires the adoption of tailor-made simplified models and experimental methodologies excluding the interference from complicating environmental factors. One approach is to examine in the isolated state the spectroscopic features of tailor-made complexes containing components which mimic the much more complicated DNA biological systems. Among the most suitable candidates, a prominent position is occupied by the (*R*)-(−)- (**Th$_R$**) and (*S*)-(+)-3-hydroxytetrahydrofuran (**Th$_S$**) enantiomers that, because of their similarity to the furanose rings of nucleotides (Figure 1), can be considered as a prototypical building block of living matter. Like many other five-membered rings, **Th$_R$** and **Th$_S$** may assume several ring-puckering conformations.[9] Besides, since they have two different functionalities, there are several different possible structures of their complexes with other molecules.[10] The first aim of the present study is to shed light on the structure acquired by either **Th$_R$** or **Th$_S$** enantiomers (henceforth denoted as **Th$_{R/S}$**) when interacting with a model chiral receptor, that is, (*R*)-(+)-1-phenyl-1-propanol (**P$_R$**), and on the nature of the noncovalent interactions holding them together in the isolated state. A second purpose is to assess the role of the asymmetric **Th$_{R/S}$** solvent molecules on the behavior of the chiral $[\mathbf{P_R}]^{\bullet+}$ radical cation. Indeed, radical ions are open-shell elusive species of paramount importance in many organic reactions and in biological processes. Oxidative bond breaking and forming involving radical ions are common processes taking place in asymmetric enzyme

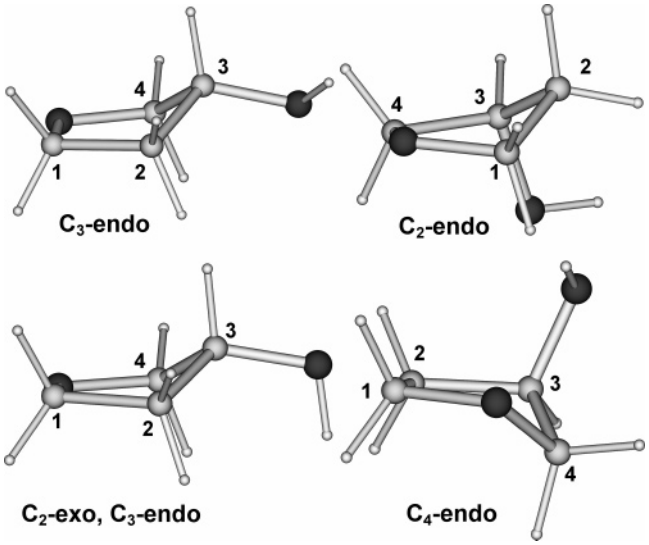


**Figure 1.** Conformational isomers of of 3-hydroxytetrahydrofuran (**Th$_{R/S}$**).

* Corresponding author. Fax: Int. Code +06-49913602. E-mail: maurizio.speranza@uniroma1.it.
[†] Università degli Studi di Roma "Tor Vergata".
[‡] Dipartimento di Chimica, Università degli Studi di Roma "La Sapienza".
[§] CNR-IMIP.
[||] Dipartimento di Studi di Chimica e Tecnologia delle Sostanze Biologicamente Attive, Università degli Studi di Roma "La Sapienza.

10.1021/jp044510h CCC: $30.25 
Published on Web 02/10/2005

cavities. Hence, knowledge of the effects of an asymmetric microenvironment on the behavior of chiral radical ions is crucial for a more exhaustive comprehension of chiral recognition and rate acceleration by enzymes. Its impact extends to another important field as well, that is, that concerning the abiogenic origin of chirality. Indeed, knowing the effects of asymmetric microsolvation on the evolution of chiral species in the isolated state may represent a key for elucidating the "chiral enrichment" mechanism of chirogenesis, that is, the preferential destruction of a specific enantiomer bound to a chiral selector.

Mass-resolved resonant two-photon ionization spectroscopy (R2PI-TOF) on a supersonically expanded molecular beam is recognized as a powerful and highly accurate tool for these purposes.[11] Supersonic beam expansion leads to the formation of isolated molecular complexes in their electronic ground state at the lowest rotational and vibrational levels. As a consequence, their excitation spectra often display only a few well-resolved peaks. Furthermore, the low internal temperature of the supersonically expanded adducts, ranging around a few kelvins,[12,13] favors population of the enthalpically most stable structural isomer and sometimes stabilization of other structural variants, if their interconversion requires the overcoming of appreciable energy barriers.

One-color R2PI (1cR2PI) experiments involve excitation of the molecular complex to its discrete $S_1$ state by the absorption of one photon of frequency $\nu_1$ and to the ionization continuum by the absorption of another photon with the same frequency, $\nu_1$. The 1cR2PI excitation spectra have been taken by recording the entire TOF mass spectrum as a function of $\nu_1$. The wavelength dependence of a given mass-resolved ion represents the excitation spectrum of the cold species and contains important information about its electronic excited state $S_1$. Two-color R2PI (2cR2PI) excitation spectra involve instead excitation of the molecular complex to its discrete $S_1$ state by the absorption of one photon of frequency $\nu_1$ and to the ionization continuum by the absorption of a second photon of a different frequency $\nu_2$. The excitation spectra of a given complex are obtained by fixing $\nu_2$ at a value slightly above the ionization threshold and by scanning $\nu_1$. In this way, no significant excess energy is imparted to the complex and decomposition of conceivable higher-order clusters is minimized. The ionization and dissociation thresholds of a given species correspond to the signal onsets obtained by scanning $\nu_2$ while keeping $\nu_1$ at the fixed value corresponding to the $S_1 \leftarrow S_0$ transition.

When a chiral chromophore, like $\mathbf{P_R}$, interacts with a chiral molecule, like $\mathbf{Th_{R/S}}$, its spectroscopic properties (including the $S_1 \leftarrow S_0$ electronic band origin) are modified to an extent which is somewhat related to the proton affinity (PA) of the molecule and the type and orientation of the functionalities involved. The first factor does not depend much on the configuration of the solvent molecule, whereas the others do.

## 2. Experimental Technique

The experimental setup for the generation of the adducts between the 3-hydroxytetrahydrofuran enantiomers ($\mathbf{Th_{R/S}}$) and (*R*)-(+)-1-phenyl-1-propanol ($\mathbf{P_R}$) and for their R2PI/TOF analysis was described previously.[12−14] Supersonic beam production of the adducts was obtained by adiabatic expansion of a carrier gas (Ar, stagnation pressure from 2 to 4 atm), seeded with $\mathbf{P_R}$ and one between $\mathbf{Th_R}$ and $\mathbf{Th_S}$ (Aldrich Chemical Co.), through a pulsed (aperture time, 200 $\mu$s; repetition rate, 10 Hz) 400 $\mu$m i.d. nozzle heated at 120 °C. In any instance, the additive concentrations were maintained low enough to minimize the contribution of heavier clusters to the spectra. The molecular beam was allowed to pass through a 1 mm skimmer into a second chamber equipped with a TOF mass spectrometer. The laser system consisted of two dye lasers pumped by a doubled Nd:YAG ($\lambda = 532$ nm). The dye fundamental frequencies were doubled and, when necessary, mixed with residual 1064 nm radiation in order to obtain two different frequencies, $\nu_1$ and $\nu_2$. The ions formed by R2PI ionization in the TOF source are mass discriminated and detected by a channeltron after a 50 cm flight path. The photoionization spectra are corrected for the effect of the electric field strength (200 V $cm^{-1}$) produced by the extraction plates of the TOF spectrometer.[13]

## 3. Computational Methods

The clusters formed by $\mathbf{P_R}$ and the selected solvent molecules are characterized by weak intermolecular forces among their functional groups. Besides, the two moieties may assume several different conformations. Therefore, the potential energy surface (PES) of their adducts is expected to be relatively flat and characterized by an ensemble of local energy minima. As a consequence, a full quantum-chemical description of the relevant PES is not feasible. Thus, the computational procedure adopted is based on a classical local energy minima search and a subsequent full quantum energetic approach.

MM3 force field classical molecular dynamics is run for each neutral adduct at a temperature of 800 K with some constraints to overcome dissociation; the cumulative time is 0.1 ns with a time step of 0.5 fs and a dump time of 1 ps. The 100 snapshots are then optimized with a convergence of $10^{-6}$ kcal/mol/Å RMS gradient per atom. The obtained optimized structures are classified according to their energy and conformation.

Each molecular and cluster conformer is optimized with a density functional theory (DFT) approach using a medium size basis set. The DFT Hamiltonian is Becke's three-parameter hybrid functional with the Lee, Yang, and Parr correlation functional; the basis set is the 6-31G** split valence plus polarization functions. The frequency calculations have been carried out in the harmonic approximation. The binding energies are computed as the difference of the total energies of the various optimized systems and corrected for the differences in the zero point energies and the basis set superposition error, as computed with the Boys and Bernardi counterpoise method.[15]

## 4. Results and Discussion

**4.1. Excitation Spectra and Structural Assignments.** Figure 2a shows the 1cR2PI ($h\nu_1 \equiv h\nu_2$) absorption spectrum of $\mathbf{P_R}$ ($[\mathbf{P_R}]^{\bullet+} = m/z$ 136). The three most intense bands have been assigned to the three stable conformers of $\mathbf{P_R}$ originating from the rotation of the ethyl group around the $C_\alpha - C_\beta$ bond.[16] The $S_1 \leftarrow S_0$ electronic origin of the most stable anti conformer and of the two gauche rotamers have been identified respectively at 37 618 (peak B), 37 577 (peak A), and 37 624 $cm^{-1}$ (peak C). Parts b and c of Figure 2 show the 1cR2PI excitation spectrum of the homochiral $[\mathbf{P_R}\cdot\mathbf{Th_R}]$ cluster and the heterochiral $[\mathbf{P_R}\cdot\mathbf{Th_S}]$ cluster, respectively, taken at *m*/*z* 195. This mass/charge ratio corresponds to the fragment arising from $C_\alpha - C_\beta$ bond fragmentation in the relevant $[\mathbf{P_R}\cdot\mathbf{Th_{R/S}}]^{\bullet+}$ species with the loss of an ethyl radical (henceforth denoted as $[(\mathbf{P_R}-C_2H_5)\cdot\mathbf{Th_{R/S}}]^+$).[17] Identical 2cR2PI excitation spectra are obtained by detecting the *m*/*z* 224 ion, corresponding to $[\mathbf{P_R}\cdot\mathbf{Th_{R/S}}]^{\bullet+}$, instead of its $[(\mathbf{P_R}-C_2H_5)\cdot\mathbf{Th_{R/S}}]^+$ fragment (*m*/*z* 195). These spectra are characterized by several bands red- (the $\alpha$ bands) or blue-shifted (the $\beta$ and $\gamma$ bands) relative to the most

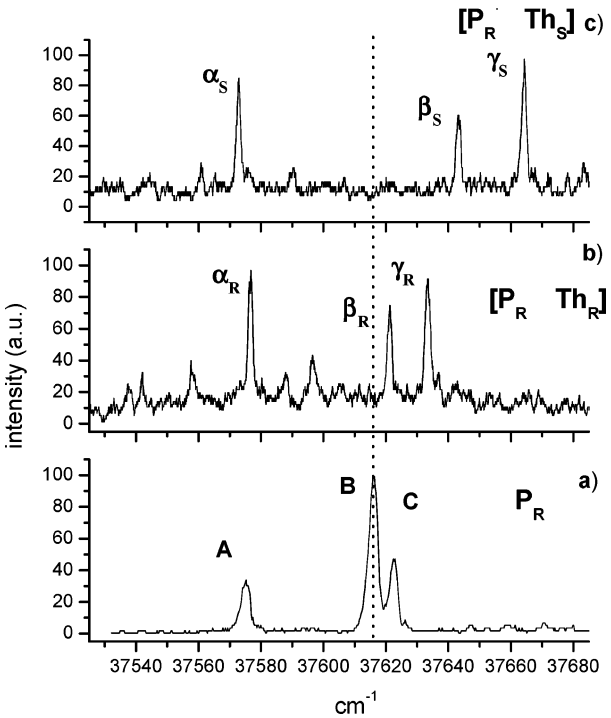


**Figure 2.** 1cR2PI excitation spectra of (*R*)-(+)-1-phenyl-1-propanol (a) and its complexes with (*R*)-(−)-3-hydroxytetrahydrofuran ([$\mathbf{P_R{\cdot}Th_R}$]) (b) and (*S*)-(+)-3-hydroxytetrahydrofuran ([$\mathbf{P_R{\cdot}Th_S}$]) (c), obtained by monitoring the ion signal at the ethyl-loss fragment mass (*m*/*z* 195). The dashed line refers to the 0° transition for the more stable anti conformer of bare $\mathbf{P_R}$.

intense band B of the bare $\mathbf{P_R}$ chromophore by the $\Delta\nu$ values reported in Table 1.

A red shift (negative $\Delta\nu$) reflects an increase of the complex bonding in going from the $S_0$ ground state to the $S_1$ excited state. A blue shift (positive $\Delta\nu$) points to a decrease of the complex bonding by the same excitation process. The magnitude of the $\Delta\nu$ values is somewhat related to the variation of bonding efficiency in the $\pi$ and $\pi^*$ states and is found to decrease in passing from the heterochiral [$\mathbf{P_R{\cdot}Th_S}$] cluster to the homochiral [$\mathbf{P_R{\cdot}Th_R}$] cluster.

As pointed out in related papers,[17,18] the red shifts of the $0_0^0$ electronic $S_1 \leftarrow S_0$ origin, observed when $\mathbf{P_R}$ is complexed with an alcohol, are phenomenologically related to the increase of the electron density on the oxygen center of the chromophore (henceforth denoted as $\mathbf{O^{chr}}$) by $\mathbf{O^{chr}}$−H···O hydrogen bonding with the O atom of the solvent.[19] Similarly important are dispersive interactions between the aliphatic chain of the alcohol and the $\pi$ system of the chromophore, which are mainly responsible for the different spectral shifts observed when also the alcoholic solvent is chiral.[18]

This general behavior is further corroborated by the 1cR2PI absorption spectra of the complexes of $\mathbf{P_R}$ with tetrahydrofuran (**Tf**) (Figure 3a) and cyclopentanol (**Cp**) (Figure 3b). Their spectral patterns are characterized by the presence of triplets of bands red-shifted relative to the $0_0^0$ electronic $S_1 \leftarrow S_0$ origins of the A−C rotamers of the bare chromophore. According to the relevant DFT computed structures and in analogy with similar assignments for [$\mathbf{P_R{\cdot}solv}$] (**solv** = secondary alcohols) complexes, the $\delta$, $\epsilon$, $\phi$ triplet of Figure 3a can be assigned to $\mathbf{O^{chr}}$−H···O bonded [$\mathbf{P_R{\cdot}Tf}$] structures with the $C_\alpha-C_\beta$ bond of the chromophore in the anti and the two gauche conformations. Analogously, the $\eta$, $\iota$, $\varphi$ triplet of Figure 3b can be assigned to the $\mathbf{O^{chr}}$−H···O bonded [$\mathbf{P_R{\cdot}Cp}$] rotamers, while the accompanying $\kappa$, $\lambda$, $\mu$ triplet can be assigned to the $\mathbf{O^{chr}}$−H···$\mathbf{O^{chr}}$ bonded [$\mathbf{P_R{\cdot}Cp}$] ones. A comparison of parts a and b of Figure 3 indicates that the magnitude of the red shifts significantly increases from the $\mathbf{O^{chr}}$−H···O bonded [$\mathbf{P_R{\cdot}Tf}$] complex to the $\mathbf{O^{chr}}$−H···O bonded [$\mathbf{P_R{\cdot}Cp}$] one, even though the gas-phase proton affinity of the two solvent molecules is very close[19] (PA(**Tf**) = 822.1 kJ mol$^{-1}$;[20] PA(**Cp**) ≥ 818 kcal mol$^{-1}$ [21]). The larger red shifts observed for the [$\mathbf{P_R{\cdot}Cp}$] complex are accounted for by the flexible cyclopentyl ring of the solvent which allows for the development of substantial dispersive interactions (see the insets of Figure 3). Similar interactions are hindered in the [$\mathbf{P_R{\cdot}Tf}$] adduct by the shorter and more rigid tetramethylenic chain of the solvent.

Complexation of $\mathbf{P_R}$ by bidentate solvent molecules, like the $\mathbf{Th_{R/S}}$ enantiomers, markedly modifies the relative population of the A−C rotamers of the chromophore.[18] Indeed, unlike the excitation spectra of the [$\mathbf{P_R{\cdot}Cp}$] and [$\mathbf{P_R{\cdot}Tf}$] complexes containing monodentate solvents, the spectral patterns of [$\mathbf{P_R{\cdot}Th_{R/S}}$] (Figure 2) exhibit both red- and blue-shifted bands, which can be hardly assigned to the $\mathbf{P_R}$ rotamers in the relevant adducts. This view is corroborated by the similarity of the HF/6-31G* computed structures of the [$\mathbf{P_R{\cdot}Th_R}$] rotamers (Figure 4) which would hardly justify the opposite band shifts of Figure 2. It is concluded that the $\alpha-\gamma$ bands of Figure 2 most likely pertain to three dominant isomeric forms of the [$\mathbf{P_R{\cdot}Th_{R/S}}$] complex characterized by different combinations of attractive forces between the two moieties.

A similar picture has been observed in previous comprehensive laser-induced fluorescence (LIF)-, UV-, and IR-dip spectroscopic studies on jet-cooled complexes of (*R*)- or (*S*)-2-naphthyl-1-ethanol ($\mathbf{N_\pm}$) with a variety of amino alcohols (**Aa**) as solvent molecules.[22−24] According to these studies, the complexes with only the most stable $\mathbf{N_\pm}$ conformer were observed experimentally. The relevant [$\mathbf{N_\pm{\cdot}Aa}$] adducts were classified into two families: (i) the "N-addition" complexes characterized by a strong $\mathbf{O^{chr}}$−H···N hydrogen bond with the most basic site of **Aa** and a much weaker O−H···$\pi$ one between the alcoholic group of **Aa** and the $\pi$ system of the chromophore and (ii) the "O-addition" complexes characterized by an intermolecular $\mathbf{O^{chr}}$−H···O hydrogen bond with the less basic site of **Aa** and by an intramolecular O−H···N hydrogen bond reinforced by the enhancement of the **Aa**'s OH acidity by the intermolecular $\mathbf{O^{chr}}$−H···O hydrogen bonding itself. The N-addition complexes were found to display red shifts much larger than those associated with the corresponding O-addition adducts. Besides the N-addition and the O-addition structures, a third [$\mathbf{Aa{\cdot}N_\pm}$] form was found to be stable on theoretical grounds. It is characterized by two very intense intermolecular $\mathbf{O^{chr}}$−H···N and O−H···$\mathbf{O^{chr}}$ interactions and was named the "insertion" complex. Despite such a strong hydrogen bond network, the insertion form was never experimentally identified among the [$\mathbf{Aa{\cdot}N_\pm}$] structures because of the relatively large deformation energy[25] (∼13 kJ mol$^{-1}$) required for inserting the OH group of the chromophore in the intramolecular hydrogen bond of the **Aa** solvent.[22−24]

As shown in Figure 1, $\mathbf{Th_{R/S}}$ presents two different basic centers, that is, the ethereal oxygen (henceforth denoted as $O^{et}$) and the alcoholic oxygen (henceforth denoted as $O^{al}$), with different affinities for the free proton (PA). DFT calculations indicate that the PA of $\mathbf{Th_{R/S}}$ at the $O^{et}$ center (PA = 861 kJ mol$^{-1}$) exceeds that at the $O^{al}$ one (PA = 831 kJ mol$^{-1}$) by ∼30 kJ mol$^{-1}$. Therefore, the $O^{et}$ atom is the most basic center in $\mathbf{Th_{R/S}}$ and plays the same role as the N atom in **Aa**. Indeed, in analogy with the [$\mathbf{N_\pm{\cdot}Aa}$] adducts, three different stable isomers have been recognized on the DFT calculated potential

**TABLE 1: R2PI Spectroscopic Parameters of Diastereomeric [$P_R$·$Th_{R/S}$] Complexes**

| complex | band | $\nu_1$ ($cm^{-1}$) | $\Delta\nu$ ($cm^{-1}$) | $^{exp}IP_{(cluster)}$[a] ($cm^{-1}$) | $^{th}\Delta D$[a] ($cm^{-1}$) | $^{exp/th}IP_{(cluster)}$[b] ($cm^{-1}$) | complex structure |
|---|---|---|---|---|---|---|---|
| [$P_R$·$Th_S$] | $\alpha_S$ | 37 573 | −45 | 70 180 | 3310 | 67 830 | $\mathbf{II}_{hetero}$ |
| | $\beta_S$ | 37 643 | +25 | 71 100 | 2641 | 68 499 | $\mathbf{I}_{hetero}$ |
| | $\gamma_S$ | 37 664 | +46 | 70 750 | 2809 | 68 331 | $\mathbf{III}_{hetero}$ |
| [$P_R$·$Th_R$] | $\alpha_R$ | 37 576 | −42 | 69 650 | 3870 | 67 270 | $\mathbf{II}_{homo}$ |
| | $\beta_R$ | 37 622 | +4 | 70 100 | 2198 | 68 942 | $\mathbf{I}_{homo}$ |
| | $\gamma_R$ | 37 634 | +16 | 69 900 | 2633 | 68 507 | $\mathbf{III}_{homo}$ |

[a] Uncertainty level: ±100 $cm^{-1}$. [b] Uncertainty level: ±140 $cm^{-1}$.

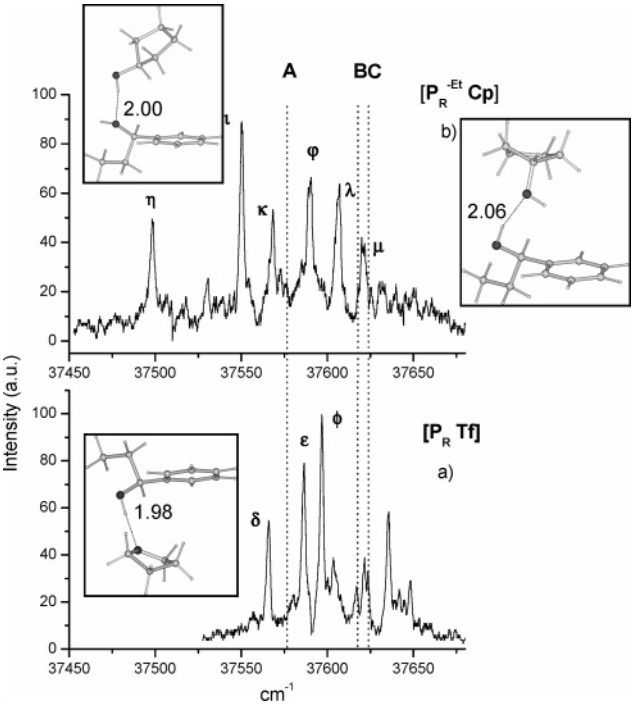


**Figure 3.** 1cR2PI excitation spectra of the complexes between (*R*)-(+)-1-phenyl-1-propanol and (a) tetrahydrofuran ([$P_R$·**Tf**]) and (c) cyclopentanol ([$P_R$·**Cp**]), obtained by monitoring the ion signal at the corresponding ethyl-loss fragment mass. The dashed line labeled B refers to the 0° transition for the more stable anti conformer of bare $P_R$. The relevant DFT computed $O^{chr}$−H···O and O−H···$O^{chr}$ structures are illustrated in the insets. The hydrogen bond distances are in angstroms.

energy surface of both the heterochiral [$P_R$·$Th_S$] and homochiral [$P_R$·$Th_R$] complexes, whose structural features are reported in Figure 5 and Table 2. Like the insertion [**Aa**·$N_\pm$] complex, structures $\mathbf{I}_{homo}$ and $\mathbf{I}_{hetero}$ present two intense intermolecular $O^{chr}$−H···$O^{et}$ and $O^{al}$−H···$O^{chr}$ interactions. Complexes $\mathbf{II}_{homo}$ and $\mathbf{II}_{hetero}$ are instead characterized by an intermolecular $O^{chr}$−H···$O^{al}$ hydrogen bond with the less basic site of $Th_{R/S}$, much like the O-addition [**Aa**·$N_\pm$] structures. Finally, structures $\mathbf{III}_{homo}$ and $\mathbf{III}_{hetero}$ exhibit an intermolecular O−H···$O^{et}$ interaction with the most basic site of $Th_{R/S}$ and a weaker $O^{al}$−H···$\pi$ one between the alcoholic group of $Th_{R/S}$ and the $\pi$ system of the chromophore, that is, a hydrogen bond arrangement somewhat resembling that of the N-addition [**Aa**·$N_\pm$] complex.

Assignment of the $\alpha-\gamma$ bands of Figure 2 to any of the three dominant [$P_R$·$Th_{R/S}$] isomeric forms of Figure 5 is by no means an easy task. A first question regards the conceivable occurrence of the insertion structures $\mathbf{I}_{homo}$ and $\mathbf{I}_{hetero}$ for the diastereomeric [$P_R$·$Th_{R/S}$] complexes. Indeed, as pointed out above, occurrence of the insertion [**Aa**·$N_\pm$] structure was prevented by the large deformation energy (~13 kJ $mol^{-1}$) accompanying insertion of the OH group of the chromophore into the strong intramolecular hydrogen bond in amino alcohols (**Aa**).[22−24] Owing to the much weaker intramolecular hydrogen bond in the $Th_{R/S}$ solvent molecule, the same insertion process is accompanied by relatively small deformation energies, that is, 5 kJ $mol^{-1}$ for [$P_R$·$Th_R$] and 7 kJ $mol^{-1}$ for [$P_R$·$Th_S$], and therefore, the insertion [$P_R$·$Th_{R/S}$] adducts may be considered as a plausible stable structure occurring in the supersonic expansion of the $P_R/Th_{R/S}$ mixtures.[25]

A criterion for the structural assignment of the $\alpha-\gamma$ bands of Figure 2b,c could be to consider the 2cR2PI appearance thresholds of the diastereomeric $[P_R\cdot Th_{R/S}]^{\bullet+}$ ions at their relevant $\alpha-\gamma$ frequencies ($^{exp}IP_{(cluster)}$ in Table 1). These phenomenological thresholds are found to increase in the following order: $^{exp}IP_{(\alpha)} < {}^{exp}IP_{(\gamma)} < {}^{exp}IP_{(\beta)}$. If this order is confronted with that of the computed $^{exp/th}IP_{(cluster)}$'s of structures **I**−**III**, one may provide a structural signature to each of the $\alpha-\gamma$ bands of Figure 2b,c. The $^{exp/th}IP_{(cluster)}$ of structures **I**−**III** can be inferred from the two equivalent expressions of their dissociative ionization potentials as reported in the two members of eq 1a. In this equation, the $^{exp}IP_{(mol)}$ term corresponds to the experimental ionization potential of the bare chromophore [$P_R$] and $^{th}D_{(cluster)}$ and $^{th}D^+_{(cluster)}$ correspond to the DFT calculated energies for the loss of $Th_{R/S}$ from the relevant $[P_R\cdot Th_{R/S}]^{\bullet+}$ and [$P_R$·$Th_{R/S}$] species. Simple rearrangement of eq 1a leads to the expression 1b for the relevant $^{exp/th}IP_{(cluster)}$ terms.

$$^{exp/th}IP_{(cluster)} + {}^{th}D^+_{(cluster)} = {}^{th}D_{(cluster)} + {}^{exp}IP_{(mol)} \quad (1a)$$

$$^{exp/th}IP_{(cluster)} = {}^{exp}IP_{(mol)} - [{}^{th}D^+_{(cluster)} - {}^{th}D_{(cluster)}] = {}^{exp}IP_{(mol)} - {}^{th}\Delta D \quad (1b)$$

The $^{exp/th}IP_{(cluster)}$ values for all **I**−**III** structures of the diasteromeric [$P_R$·$Th_{R/S}$] pairs are reported in Table 1. The evident discrepancy between the experimental $^{exp}IP_{(cluster)}$ values and the corresponding calculated $^{exp/th}IP_{(cluster)}$ ones may be attributed to computational systematic errors or, more likely, to the operation of the Franck−Condon (FC) effect on the $^{exp}IP_{(cluster)}$ measurement. However, given the similar structural distortions accompanying **I**−**III** ionization (Figure 5), it is plausible that comparable FC effects operate in the process. In this frame, the phenomenological $^{exp}IP_{(\alpha)} < {}^{exp}IP_{(\gamma)} < {}^{exp}IP_{(\beta)}$ order can be properly confronted with the calculated $^{exp/th}IP_{(\mathbf{II})} < {}^{exp/th}IP_{(\mathbf{III})} < {}^{exp/th}IP_{(\mathbf{I})}$ one (Table 1). The resulting qualitative agreement permits structure **II** to be assigned safely to the $\alpha$ bands, whereas no definitive conclusions can be drawn on these grounds about the structural signature of the $\beta$ and $\gamma$ bands. The $\alpha \leftrightarrow$ **II** matching is further corroborated by the following circumstantial evidence. Close inspection of the DFT calculated "$O^{al}$-addition" structure $\mathbf{II}_{hetero}$ (Table 2 and Figure 5) points to the presence of both an intermolecular $O^{chr}$−H···$O^{al}$ hydrogen bond (hydrogen bond distance = 1.89 Å) and an intramolecular $O^{al}$−H···$O^{et}$ interaction (hydrogen bond distance = 2.50 Å). Its $\mathbf{II}_{homo}$ diastereomer is instead characterized by comparatively weaker $O^{chr}$−H···$O^{al}$ hydrogen bonding (hydrogen bond distance = 1.92 Å) and $O^{al}$−H···$O^{et}$ intramolecular interaction

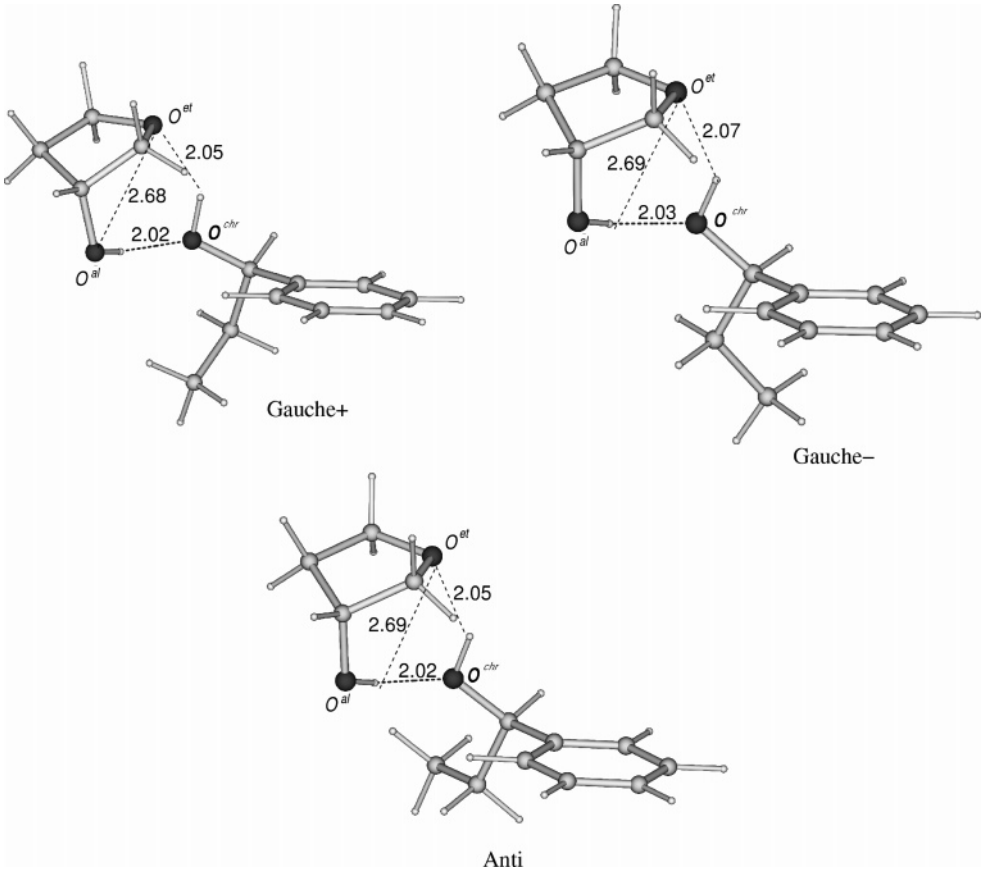


**Figure 4.** HF/6-31G* calculated [$\mathbf{P_R}\cdot\mathbf{Th_R}$] equilibrium structures obtained for all three rotamers of the chromophore. The hydrogen bond distances are in angstroms.

(hydrogen bond distance = 2.57 Å). It is therefore expected that those intracomplex interactions that in $\mathbf{II}_{hetero}$ are responsible for the red shift of the $\alpha_S$ band must be slightly weakened in $\mathbf{II}_{homo}$ and, therefore, lead to a less-red-shifted absorption band. Accordingly, $\mathbf{II}_{homo}$ should display a red shift lower than that of $\mathbf{II}_{hetero}$, as actually observed only for the corresponding α bands (Figure 2b,c). Concerning the structural assignment of the $\beta$ and $\gamma$ bands, Table 2 shows that the diastereomeric "$O^{et}$-addition" structures **III** exhibit an appreciable weakening of intramolecular $O^{al}-H\cdots O^{et}$ bonding (hydrogen bond distance = 2.67 Å ($\mathbf{III}_{homo}$); 2.68 Å ($\mathbf{III}_{hetero}$)) relative to that in the isolated $\mathbf{Th_{R/S}}$ (hydrogen bond distance = 2.47 Å) which is essentially replaced by an $O^{al}-H\cdots\pi$ interaction between the OH group of $\mathbf{Th_{R/S}}$ and the $\pi$ system of the chromophore (hydrogen bond distance = 2.95 Å ($\mathbf{III}_{homo}$); 3.06 Å ($\mathbf{III}_{hetero}$); Table 2). This may account for the large blue shifting of the $\gamma$ band relative to the $0_0^0$ electronic $S_1 \leftarrow S_0$ origin of the B rotamer of the bare chromophore.[28] It should also be pointed out in this connection that, despite the shorter $O^{al}-H\cdots\pi$ distance, $\mathbf{III}_{homo}$ shows a smaller blue shift relative to $\mathbf{III}_{hetero}$. This effect is to be ascribed to the more effective dispersive interactions in $\mathbf{III}_{homo}$ (Figure 5) which partly counterbalance the $\pi$ electron withdrawing action of the $O^{al}-H\cdots\pi$ bonding. Taking for granted the peak α ↔ **II** and peak $\gamma$ ↔ **III** assignments, peaks $\beta$ of Figure 2 are necessarily associated with the corresponding insertion structures **I** by exclusion. This assignment conforms as well to the smallest shift of the $\beta$ bands relative to the $0_0^0$ electronic $S_1 \leftarrow S_0$ origin of the B form of the bare chromophore which probably reflects a sort of "compensation" by the proton-donating $\mathbf{O^{chr}}-H\cdots O^{et}$ and proton-accepting $O^{al}-H\cdots\mathbf{O^{chr}}$ effects on the $S_1 \leftarrow S_0$ transition for the insertion structures **I** (cfr. the relevant hydrogen bond distances in Table 2). Other circumstantial evidence in favor of the above assignments will be given in the following section.

**4.2. Ionization and Fragmentation Processes.** This section is devoted to the evaluation of the effects of the asymmetric $\mathbf{Th_R}$ and $\mathbf{Th_S}$ solvent molecules containing two different basic centers, that is, $O^{et}$ and $O^{al}$, on the side-chain $C_\alpha-C_\beta$ bond cleavage in the relevant $[\mathbf{P_R}\cdot\mathbf{Th_{R/S}}]^{\bullet+}$ adducts (eqs 2 and 3).

$$\text{Ionization: } [\mathbf{P_R}\cdot\mathbf{Th_{R/S}}] + h\nu_1 \rightarrow [\mathbf{P_R}\cdot\mathbf{Th_{R/S}}]^* + h\nu_2 \rightarrow [\mathbf{P_R}\cdot\mathbf{Th_{R/S}}]^{\bullet+} + e \quad (2)$$

$$\text{Fragmentation: } [\mathbf{P_R}\cdot\mathbf{Th_{R/S}}]^{\bullet+} \rightarrow [(\mathbf{P_R}-C_2H_5)\cdot\mathbf{Th_{R/S}}]^{+} + {}^{\bullet}C_2H_5 \quad (3)$$

The overall energy of sequence 2−3 can be expressed by the corresponding phenomenological threshold $^{exp}AE^{-Et}$ (Table 3 and Figure 6). Its value spans over a limited energy range from 71 585 to 72 435 $cm^{-1}$ for $[\mathbf{P_R}\cdot\mathbf{Th_S}]$ and from 71 385 to 72 500 $cm^{-1}$ for $[\mathbf{P_R}\cdot\mathbf{Th_R}]$. Besides, the energy range is even narrower when comparing the diastereomeric pairs $\mathbf{I}_{hetero}/\mathbf{I}_{homo}$, $\mathbf{II}_{hetero}/\mathbf{II}_{homo}$, and $\mathbf{III}_{hetero}/\mathbf{III}_{homo}$, with the major $^{exp}AE^{-Et}$ difference being observed for the latter (225 $cm^{-1}$). The $^{exp}AE^{-Et}$ thresholds of Table 3 are measured relative to the ground state of the pertinent isomeric structures **I**−**III**. To estimate the minimum total energy ($\Delta E^{\ddagger}$ in Figure 6) of structures **I**−**III** when undergoing $C_\alpha-C_\beta$ bond fragmentation, the DFT calculated stability gap of each isomeric structure relative to the most stable one $\mathbf{I}_{homo}$ ($^{th}\Delta E_0$ in Figure 6) has been added to the experimental $^{exp}AE^{-Et}$ terms. The $\Delta E^{\ddagger} = {}^{exp}AE^{-Et} + {}^{th}\Delta E_0$ terms, obtained in this way, tend to cluster around the same value (72 400 ± 160; Table 3), thus suggesting that any adduct,

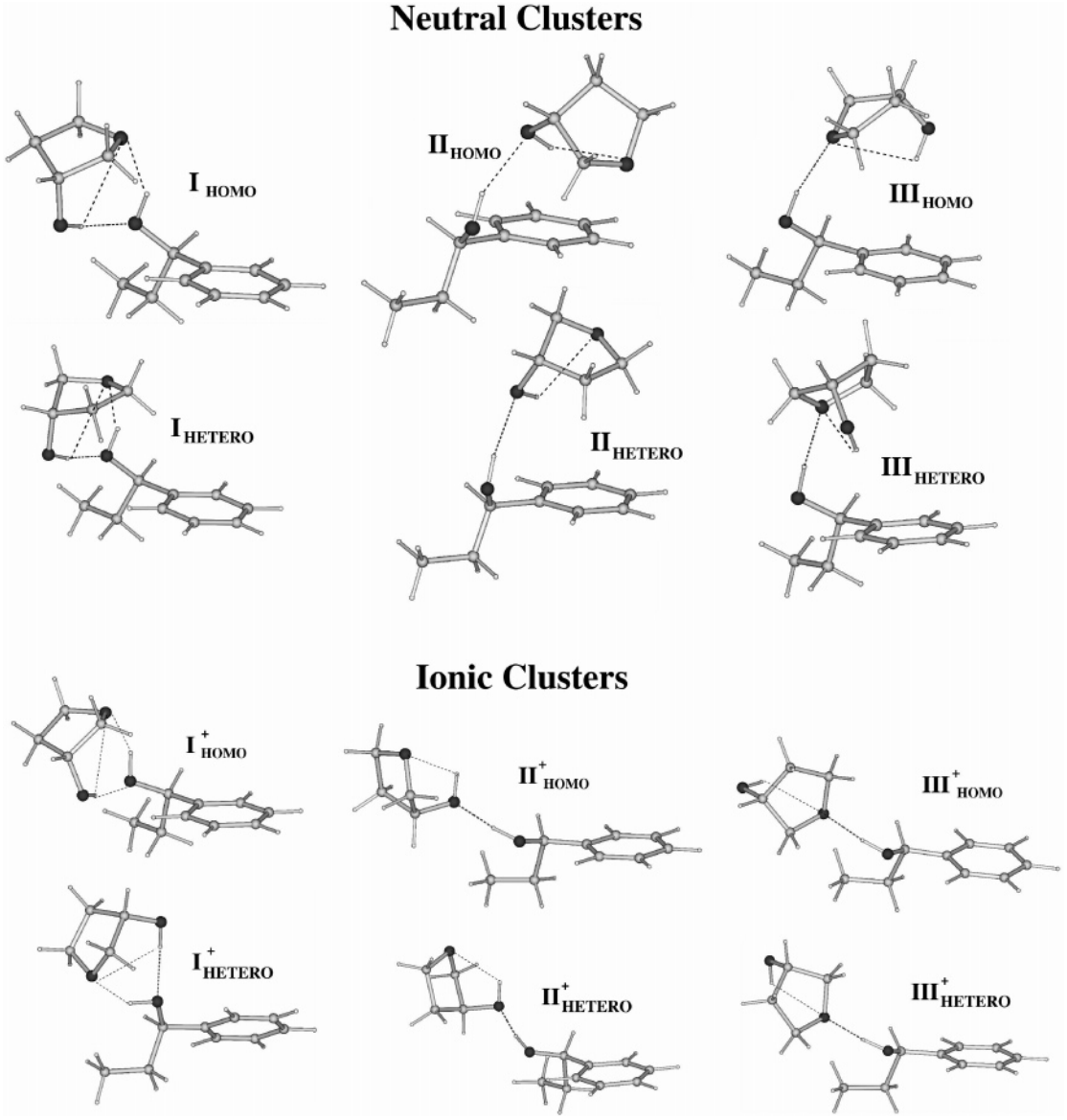


**Figure 5.** DFT calculated [$\mathbf{P_R \cdot Th_{R/S}}$] and [$\mathbf{P_R \cdot Th_{R/S}}$]$^{\bullet+}$ equilibrium isomeric structures.

**TABLE 2: Hydrogen Bond Distances (Å)**

| species | structure | $O^{al}-H\cdot\cdot\cdot O^{et}$ | $\mathbf{O^{chr}}-H\cdot\cdot\cdot O$ | $O-H\cdot\cdot\cdot\mathbf{O^{chr}}$ | $O^{al}-H\cdot\cdot\cdot\pi^a$ |
|---|---|---|---|---|---|
| [$\mathbf{Th_{R/S}}$] | $C_4$-endo | 2.47 | | | |
| [$\mathbf{P_R \cdot Th_R}$] | $\mathbf{I}_{homo}$ | 2.75 | 1.87 | 1.86 | 4.41 |
| | $\mathbf{II}_{homo}$ | 2.57 | 1.92 | | 3.16 |
| | $\mathbf{III}_{homo}$ | 2.67 | 1.89 | | 2.95 |
| [$\mathbf{P_R \cdot Th_S}$] | $\mathbf{I}_{hetero}$ | 2.74 | 1.87 | 1.84 | 4.34 |
| | $\mathbf{II}_{hetero}$ | 2.50 | 1.89 | | 3.19 |
| | $\mathbf{III}_{hetero}$ | 2.68 | 1.88 | | 3.06 |
| [$\mathbf{P_R \cdot Th_R}$]$\bullet^+$ | $\mathbf{I}^{\bullet+}_{homo}$ | 2.76 | 1.86 | 1.80 | 4.45 |
| | $\mathbf{II}^{\bullet+}_{homo}$ | 2.30 | 1.64 | | 6.26 |
| | $\mathbf{III}^{\bullet+}_{homo}$ | 2.64 | 1.64 | | 8.35 |
| [$\mathbf{P_R \cdot Th_S}$]$^{\bullet+}$ | $\mathbf{I}^{\bullet+}_{hetero}$ | 2.70 | 1.90 | 1.82 | 4.57 |
| | $\mathbf{II}^{\bullet+}_{hetero}$ | 2.30 | 1.65 | | 6.25 |
| | $\mathbf{III}^{\bullet+}_{hetero}$ | 2.63 | 1.64 | | 8.11 |
| [($\mathbf{P_R}-C_2H_5$)$\cdot\mathbf{Th_R}$]$^+$ | from $\mathbf{II}^{\bullet+}$ | 2.24 | 1.43 | | 6.48 |
| | from $\mathbf{I}^{\bullet+}/\mathbf{III}^{\bullet+}$ | 3.82 | 1.36 | | 9.58 |
| [($\mathbf{P_R}-C_2H_5$)$^{\bullet+}\cdot\mathbf{Th_S}$]$^{\bullet}$ | from $\mathbf{II}^{\bullet+}$ | 2.29 | 1.55 | | 6.54 |
| | from $\mathbf{I}^{\bullet+}/\mathbf{III}^{\bullet+}$ | 3.82 | 1.52 | | 9.59 |

[a] The $O^{al}-H\cdot\cdot\cdot\pi$ distance refers to the center of the aromatic ring.

irrespective of its structure, must attain almost the same energy level to undergo $C_\alpha-C_\beta$ bond fragmentation. This level is probably determined by the crossing between the PES adiabatically correlated with the open-shell biradical cation [($\mathbf{P_R}-C_2H_5$)$^{\bullet+}\cdot\mathbf{Th_{R/S}}$]$^{\bullet}$ and the PES adiabatically correlated with the closed-shell cation [($\mathbf{P_R}-C_2H_5$)$\cdot\mathbf{Th_{R/S}}$]$^+$ (Figure 6).[26,27,29] In this connection, the differences in the total energies ($\Delta\Delta E^{\ddagger}$) (Table 3 and Figure 6) correspond to the energy gaps between the

**TABLE 3: Ethyl-Loss Fragmentation Thresholds and Activation Energies for the Ethyl Radical Loss from the $[P_R \cdot solv]^{\bullet+}$ Ions**

| ionic species | isomeric structure | $^{exp}AE^{-Et}$ [a] ($cm^{-1}$) | $^{th}\Delta E_0$ [a] ($cm^{-1}$) | $\Delta E^{\ddagger} = {}^{exp}AE^{-Et} + {}^{th}\Delta E_0$ ($cm^{-1}$) | $\Delta\Delta E^{\ddagger}$ ($cm^{-1}$) | $E_{act}$ [b] ($cm^{-1}$) | $\Delta E_+$ [a] ($cm^{-1}$) |
|---|---|---|---|---|---|---|---|
| $[P_R \cdot Th_R]$ | $I_{homo}$ | 72 500 | 0 | 72 500 | +262 | 3558 | 819 |
| | $II_{homo}$ | 71 385 | +853 | 72 238 | 0 | 4115 | 0 |
| | $III_{homo}$ | 72 185 | +368 | 72 553 | +315 | 3678 | 752 |
| $[P_R \cdot Th_S]$ | $I_{hetero}$ | 72 435 | +159 | 72 594 | +356 | 3936 | 535 |
| | $II_{hetero}$ | 71 585 | +685 | 72 270 | +32 | 3755 | 392 |
| | $III_{hetero}$ | 71 960 | +343 | 72 303 | +65 | 3629 | 552 |

[a] Uncertainty level: $\pm 100$ $cm^{-1}$. [b] $E_{act} = {}^{exp}AE^{-Et} - {}^{exp/th}IP_{(cluster)}$, uncertainty level: $\pm 140$ $cm^{-1}$.

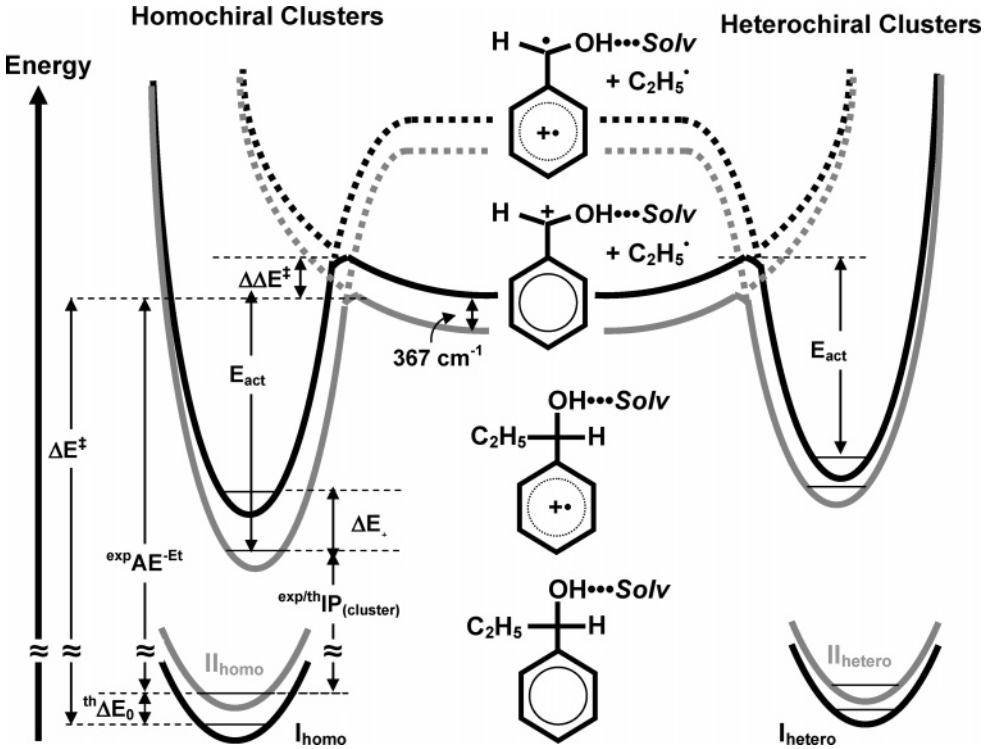


**Figure 6.** Schematic representation of the potential energy curves for isomers **I** (black lines) and **II** (grey lines) of the homochiral $[P_R \cdot Th_R]$ complex (left) and the heterochiral $[P_R \cdot Th_S]$ complex (right). The curves relative to structures **III** are similar to those of **II** and are omitted for the sake of clarity. The potential wells and the dissociation limits refer to the species shown in the center of the figure.

transition structures for the side-chain $C_\alpha - C_\beta$ bond cleavage in the corresponding $I^{\bullet+} - III^{\bullet+}$ isomers. Taking into account that the DFT computed energy gap between the $O^{chr}-H\cdot\cdot\cdot O^{et}$ bonded $[(P_R - C_2H_5) \cdot Th_{R/S}]^+$ fragment formed from $I^{\bullet+}$ or $III^{\bullet+}$ and the more stable $O^{chr}-H\cdot\cdot\cdot O^{al}$ bonded $[(P_R - C_2H_5) \cdot Th_{R/S}]^+$ fragment arising from $II^{\bullet+}$ is 367 $cm^{-1}$, one would expect that the relevant $\Delta\Delta E^{\ddagger}$ terms do not exceed this limit (Figure 6).[29] This is indeed the case with the peak $\alpha \leftrightarrow$ **II**, peak $\beta \leftrightarrow$ **I**, and peak $\gamma \leftrightarrow$ **III** matching. Any other combination would give $\Delta\Delta E^{\ddagger} \gg 367$ $cm^{-1}$ in clear contrast with the expectation.

Table 3 reports the activation energies ($E_{act}$) for the fragmentation step 3 for each $[P_R \cdot Th_{R/S}]^{\bullet+}$ structure estimated from the difference between the relevant $^{exp}AE^{-Et}$ terms and $^{exp/th}IP_{(cluster)}$ terms (Table 1). The same table gives also the DFT computed relative energies ($\Delta E_+$) of the corresponding $[P_R \cdot Th_{R/S}]^{\bullet+}$ isomeric structures (Figure 6). Comparison between the relevant $E_{act}$ and $\Delta E_+$ sets of data confirms previous views about the existence of an inverse relationship between them.[26,27] For all $[P_R \cdot Th_R]^{\bullet+}$ isomers and for structures $II_{hetero}$ and $III_{hetero}$ of $[P_R \cdot Th_S]^{\bullet+}$, the greater the stability of the ionic adducts, the greater is its phenomenological fragmentation barrier ($E_{act}$).[26,27] This means that the energy gap of 367 $cm^{-1}$ between the $O^{chr}-H\cdot\cdot\cdot O^{et}$ bonded $[(P_R - C_2H_5) \cdot Th_{R/S}]^+$ fragment and the more stable $O^{chr}-H\cdot\cdot\cdot O^{al}$ bonded one (Figure 6) plays only a minor role in determining the $\Delta\Delta E^{\ddagger}$ differences, the major role being played by the much greater $\Delta E_+$ ion stability differences (Table 3).

$E_{act}$ of the $II_{hetero}$ structure of $[P_R \cdot Th_S]^{\bullet+}$ does not follow the same trend. This can be attributed to the fact that, at variance with what was observed for the homochiral $[P_R \cdot Th_R]^{\bullet+}$ isomers, the $\Delta E_+$ differences for the heterochiral $[P_R \cdot Th_S]^{\bullet+}$ structures ($\Delta E_+(I_{hetero}) - \Delta E_+(II_{hetero}) = 143$ $cm^{-1}$; $\Delta E_+(I_{hetero}) - \Delta E_+(III_{hetero}) = -17$ $cm^{-1}$) are much narrower than those between the corresponding $\Delta\Delta E^{\ddagger}$ values ($\Delta\Delta E^{\ddagger}(I_{hetero}) - \Delta\Delta E^{\ddagger}(II_{hetero}) = 324$ $cm^{-1}$; $\Delta\Delta E^{\ddagger}(I_{hetero}) - \Delta\Delta E^{\ddagger}(III_{hetero}) = 291$ $cm^{-1}$). These findings would suggest that the $\Delta\Delta E^{\ddagger}$ differences for the heterochiral $[P_R \cdot Th_S]^{\bullet+}$ structures are influenced not only by the stability of the relevant ionic adducts but also by the stability difference between the $O^{chr}-H\cdot\cdot\cdot O^{et}$ bonded $[(P_R - C_2H_5) \cdot Th_{R/S}]^+$ fragment and the more stable $O^{chr}-H\cdot\cdot\cdot O^{al}$ bonded one (Figure 6).

## 5. Conclusions

Mass-resolved R2PI spectroscopy coupled with high-level ab initio calculations provides valuable insights into the interactive forces involved in the complexation of $P_R$ by the two enantiomers of 3-hydroxytetrahydrofuran ($Th_{R/S}$). Three different hydrogen bonded $[P_R \cdot Th_{R/S}]$ isomers have been recovered in

the supersonic expansion of the relevant components wherein the $\mathbf{P_R}$ chromophore is (i) either a hydrogen bond donor and hydrogen bond acceptor toward the OH group of $\mathbf{Th_{R/S}}$ (structure **I**), (ii) a hydrogen bond donor to the OH group of $\mathbf{Th_{R/S}}$ (structure **II**), or (iii) a hydrogen bond donor to the ethereal O atom of $\mathbf{Th_{R/S}}$ and O−H···$\pi$ bond acceptor from the solvent molecule (structure **III**). Diastereomeric structures **II** exhibit a batochromic shift of their $S_1 \leftarrow S_0$ electronic band origin relative to that of the most stable anti conformer of the bare $\mathbf{P_R}$ chromophore to an extent which slightly increases with the strength of the intermolecular hydrogen bonding. Diastereomeric structures **III** display instead an ipsochromic shift due primarily to the intermolecular O−H···$\pi$ bonding whose extent is appreciably affected by secondary dispersive interactions between the chromophore and the solvent. Finally, the diastereomeric structures **I** show the smallest band shifts due to the dual hydrogen bond donor/acceptor character of the chromophore. In all instances, the different shifts of the band origin region observed for the diastereomeric [$\mathbf{P_R}$·$\mathbf{Th_S}$] and [$\mathbf{P_R}$·$\mathbf{Th_R}$] complexes provide a viable means for spectroscopically discriminating the $\mathbf{Th_{R/S}}$ enantiomers.

A further tool for their differentiation is provided by the 2cR2PI-TOF measurement of the phenomenological activation barriers for the homolytic $C_\alpha-C_\beta$ bond cleavage in the [$\mathbf{P_R}$·$\mathbf{Th_S}$]$^{\bullet+}$ and [$\mathbf{P_R}$·$\mathbf{Th_R}$]$^{\bullet+}$ radical cations arising from photoionization of the corresponding diastereomeric [$\mathbf{P_R}$·$\mathbf{Th_S}$] and [$\mathbf{P_R}$·$\mathbf{Th_R}$] complexes. A direct relationship is found between the stability of the homochiral [$\mathbf{P_R}$·$\mathbf{Th_R}$]$^{\bullet+}$ isomers and the relevant fragmentation barriers. No similar relationship is observed for the heterochiral [$\mathbf{P_R}$·$\mathbf{Th_S}$]$^{\bullet+}$ structures. For these systems, which are characterized by limited stability differences, the phenomenological activation barriers for the homolytic $C_\alpha-C_\beta$ bond cleavage are influenced by the relative stability of the fragmentation products as well.

**Acknowledgment.** This work was supported by the Ministero della Università e della Ricerca Scientifica e Tecnologica (MURST) and the Consiglio Nazionale delle Ricerche (CNR).

## References and Notes

(1) Saenger, W. *Principles of Nucleic Acid Structure*; Springer-Verlag: New York, 1984.
(2) Franklin, R. E.; Gosling, R. *Nature* **1953**, *171*, 740.
(3) Leslie, A. G. W.; Arott, S.; Chandrasekaran, R.; Ratliff, R. L. *J. Mol. Biol.* **1980**, *143*, 49.
(4) Luger, K.; Mäder, A. W.; Richmond, R. K.; Sargent, D. F.; Richmond, J. T. *Nature* **1997**, *389*, 251.
(5) Klimasauskas, S.; Kumar, S.; Roberts, R. J.; Cheng, X. *Cell* **1994**, *76*, 357.
(6) Roberts, R. J. *Cell* **1995**, *82*, 9.
(7) Slupphaug, G.; Mol, C. D.; Kavli, B.; Arvai, A. S.; Krokan, H. E.; Tainer, J. A. *Nature* **1996**, *71*, 3344.
(8) Takahara, P. M.; Rosenzweig, A. C.; Frederick, C. A.; Lippard, J. S. *Nature* **1995**, *377*, 649.
(9) Lavrich, R. J.; Rhea, R. L.; McCargar, J. W.; Tubergen, M. J. *J. Mol. Spectrosc.* **2000**, *199*, 138.
(10) Lavrich, R. J.; Torok, C. R.; Tubergen, M. J. *J. Phys. Chem. A* **2001**, *105*, 8317.
(11) Speranza, M.; Satta, M.; Piccirillo, S.; Rondino, F.; Paladini, A.; Giardini, A.; Filippi, A.; Catone, D. *Mass Spectrom. Rev.*, in press .
(12) Piccirillo, S.; Coreno, M.; Giardini-Guidoni, A.; Pizzella, G.; Snels, M.; Teghil, R. *J. Mol. Struct.* **1993**, *293*, 197.
(13) Di Palma, T. M.; Latini, A.; Satta, M.; Varvesi, M.; Giardini Guidoni, A. *Chem. Phys. Lett.* **1998**, *284*, 184.
(14) Consalvo, D.; van der Avoird, A.; Piccirillo, S.; Coreno, M.; Giardini-Guidoni, A.; Mele, A.; Snels, M. *J. Chem. Phys.* **1993**, *99*, 8398.
(15) Boys, S. F.; Bernardi, F. *Mol. Phys.* **1970**, *19*, 553.
(16) Latini, A.; Satta, M.; Giardini Guidoni, A.; Piccirillo, S.; Speranza, M. *Chem.—Eur. J.* **2000**, *6*, 6.
(17) Giardini-Guidoni, A.; Piccirillo, S.; Palleschi, A.; Toja, D. *Proc.—Indian Acad. Sci., Chem. Sci.* **1998**, *110*, 153.
(18) Scuderi, D.; Paladini, A.; Piccirillo, S.; Satta, M.; Catone, D.; Giardini, A.; Filippi, A.; Speranza, M. *Chem. Commun.* **2002**, 2438.
(19) In general, the hydrogen bond strength increases with the acidity of the donor ($\Delta H°_{acid}$) and the proton affinity (PA) of the acceptor (Hibbert, F.; Emsley, J. *Adv. Phys. Org. Chem.* **1990**, *26*, 225).
(20) http://webbook.nist.gov./chemistry/.
(21) Estimated from the PA limits of secondary alcohols (Long, J.; Munson, B. *J. Am. Chem. Soc.* **1977**, *99*, 6822), using the group additivity method (Benson, S. W. *Thermochemical Kinetics*; Wiley: New York, 1968).
(22) Le Barbu, K.; Lahmani, F.; Zehnacker-Rentien, A. *J. Phys. Chem. A* **2002**, *106*, 6271.
(23) Seurre, N.; Le Barbu-Debus, K.; Lahmani, F.; Zehnacker-Rentien, A.; Sepiol, J. *J. Mol. Struct.* **2004**, *692*, 127.
(24) Seurre, N.; Sepiol, J.; Le Barbu-Debus, K.; Lahmani, F.; Zehnacker-Rentien, A. *Phys. Chem. Chem. Phys.* **2004**, *6*, 2867.
(25) The deformation energy is defined as the difference between the energy of the molecular components within the complex and in their most stable conformation as isolated subunits.
(26) Catone, D.; Giardini Guidoni, A.; Paladini, A.; Piccirillo, S.; Rondino, F.; Satta, M.; Scuderi, D.; Speranza, M. *Angew. Chem., Int. Ed.* **2004**, *43*, 1868.
(27) Piccirillo, S.; Satta, M.; Catone, D.; Scuderi, D.; Paladini, A.; Rondino, F.; Speranza, M.; Giardini Guidoni, A. *Phys. Chem. Chem. Phys.* **2004**, *10*, 2858.
(28) Similar blue shifts have been observed with the [$\mathbf{P_R}$·$H_2O$] complexes; cfr. Satta, M.; Latini, A.; Piccirillo, S.; Di Palma, T. M.; Scuderi, D.; Speranza, M.; Giardini, A. *Chem. Phys. Lett.* **2000**, *316*, 94.
(29) The PES adiabatically correlated with the open-shell biradical cation [($\mathbf{P_R}$−$C_2H_5$)$^{\bullet+}$·$\mathbf{Th_{R/S}}$]$^\bullet$ is expected to be rather insensitive to the configuration and the orientation ($\mathbf{O^{chr}}$−H···$O^{al}$ vs $\mathbf{O^{chr}}$−H···$O^{et}$) of the $\mathbf{Th_{R/S}}$ solvent. A reason for this can be found in the significant distance between the solvent dipole and the electron vacancy formally located on the $\pi$ system of the chromophore in the open-shell biradical cation [($\mathbf{P_R}$−$C_2H_5$)$^{\bullet+}$·$\mathbf{Th_{R/S}}$]$^\bullet$. As a consequence, the energy gap between the transition structures for the side-chain $C_\alpha-C_\beta$ bond cleavage in the corresponding $\mathbf{I}^{\bullet+}$−$\mathbf{III}^{\bullet+}$ isomers is essentially correlated to the energy difference of 367 cm$^{-1}$ between the $\mathbf{O^{chr}}$−H···$O^{et}$ bonded [($\mathbf{P_R}$−$C_2H_5$)·$\mathbf{Th_{R/S}}$]$^+$ fragment arising from $\mathbf{I}^{\bullet+}$ or $\mathbf{III}^{\bullet+}$ and the more stable $\mathbf{O^{chr}}$−H···$O^{al}$ bonded [($\mathbf{P_R}$−$C_2H_5$)·$\mathbf{Th_{R/S}}$]$^+$ fragment arising from $\mathbf{II}^{\bullet+}$.